Published in final edited form as:
Structure. 2013 May 7; 21(5): 707–717. doi:10.1016/j.str.2013.03.003.

Structure and T-cell inhibition properties of B7 family member, B7-H3

Vladimir Vigdorovich[1,*], **Udupi A. Ramagopal**[2], **Eszter Lázár-Molnár**[1], **Eliezer Sylvestre**[1], **Jun Sik Lee**[1,‡], **Kimberly A. Hofmeyer**[1], **Xingxing Zang**[1], **Stanley G. Nathenson**[1,3], and **Steven C. Almo**[2,4,*]

[1]Department of Microbiology & Immunology, Albert Einstein College of Medicine, Bronx, NY 10461, USA

[2]Department of Biochemistry, Albert Einstein College of Medicine, Bronx, NY 10461, USA

[3]Department of Cell Biology, Albert Einstein College of Medicine, Bronx, NY 10461, USA

[4]Department of Physiology & Biophysics, Albert Einstein College of Medicine, Bronx, NY 10461, USA

Summary

T-cell activity is controlled by a combination of antigen-dependent signaling through the T-cell receptor and a set of auxiliary signals delivered through antigen-independent interactions, including the recognition of the B7 family of ligands. B7-H3 is a recently identified B7 family member that is strongly overexpressed in a range of cancers and correlates with poor prognosis. We report the crystal structure of murine B7-H3 at a 3-Å resolution, which provides a model for the organization of the IgV and IgC domains within the ectodomain. We demonstrate that B7-H3 inhibits T-cell proliferation and show that the FG loop of the IgV domain plays a critical role in this function. B7-H3 crystallized as an unusual dimer arising from the exchange of the G strands in the IgV domains of partner molecules. This arrangement, in combination with previous reports, highlights the dynamic nature and plasticity of the immunoglobulin fold.

Introduction

T-cell activity is controlled by the integration of signals arising from multiple molecular interactions on the cell surface. According to the canonical two-signal model, engagement between the T-cell receptor (TCR) and the antigenic peptide:major histocompatibility complex (pMHC) displayed on the surface of the antigen-presenting cell (APC) (i.e., “signal 1”) is essential but not sufficient for activation of naïve T cells *in vivo*. This antigen-dependent signal requires additional antigen-independent signals, which can either lead to

*corresponding author: steve.almo@einstein.yu.edu, 718-430-2746 (phone), 718-430-8565 (fax), vladimir.vigdorovich@gmail.com.
‡current affiliation: Department of Biology, College of Natural Science, Chosun University, Gwangju, 501-757, Korea

activation of T cells (e.g., through formation of CD28:B7 complexes) or to down-regulation of their activity (e.g., through the formation of CTLA-4:B7 complexes).

The identification of the crucial costimulatory signal through the CD28 receptor was prompted by the observation that in absence of B7-1 or B7-2 on the APC, engagement of the TCR on naïve T cells causes them to become non-responsive (i.e., anergic) (Sharpe and Freeman, 2002). Once activated, T cells express the inhibitory CTLA-4 receptor, which also binds (and, thus, competes with CD28 for) the B7-1 and B7-2 ligands, providing a control mechanism for T-cell proliferation (Sharpe and Freeman, 2002). Additional sequence-related molecules have since been identified and characterized as leading to stimulation (e.g., ICOSL) or inhibition (e.g., PD-L1, PD-L2) of T-cell activity via engagement of their corresponding receptors (ICOS and PD-1, respectively), thereby defining the B7 family of proteins (Sharpe and Freeman, 2002). B7 family members belong to the immunoglobulin superfamily and, while sharing low sequence identity, have a common domain structure and interact with receptors belonging to the CD28 protein family (Sharpe and Freeman, 2002; Hansen et al., 2009). *In vivo*, tissue localization and timing of expression of these molecules provide mechanisms for the fine-tuning of T-cell activity in response to a wide range of immune challenges.

B7-H3 is a recently recognized member of the B7 family. Like other members, murine B7-H3 is a type-1 transmembrane protein possessing an ectodomain composed of a single IgV-IgC domain pair with the overall sequence identity of ≤30%, when compared to the other B7 family members. In the mouse, B7-H3 transcripts are found in a variety of tissues, including brain, lung, colon, kidney and spleen (Sun et al., 2002; Ling et al., 2003; Sun et al., 2003). Although initially identified as an activator of T-cell function (Chapoval et al., 2001), subsequent reports have shown that B7-H3 can lead to downregulation of T-cell activity (Suh et al., 2003; Prasad et al., 2004).

B7-H3 protein is normally found at low levels in many healthy tissues as well as on activated cells of the immune system, and has been reported to be strongly overexpressed in a wide variety of human malignancies (Zang et al., 2007; Yamato et al., 2009; Barach et al., 2010; Crispen et al., 2008; Roth et al., 2007; Loos et al., 2010)—a scenario associated with poor clinical outcomes. In particular, 93% of prostate cancers overexpress B7-H3 and patients with higher levels of B7-H3 on tumor cells are significantly more likely to exhibit disseminated disease at the time of surgery, increased recurrence and higher mortality (Zang et al., 2007). In addition to cancer cells, B7-H3 is also expressed in the endothelium of cancer-associated vasculature in 44% of ovarian cancer patients, which is associated with a significantly shorter survival time and a higher incidence of recurrence (Zang et al., 2010). These findings, together with the ability of B7-H3 to inhibit the activity and proliferation of T cells, suggest that tumor cells use the signal delivered by B7-H3 to evade anti-tumor immunity. The potential role in immune evasion makes B7-H3 a compelling target for anticancer therapy.

We report the crystal structure of the extracellular domain of murine B7-H3 (mB7H3), which reveals an unusual organization involving a strand swap between the dimer-forming IgV domains. Based on this structure, a model of B7-H3 with canonical interactions between

the IgV and IgC domains was constructed and used as the basis for mutagenesis studies that revealed a critical role for the FG loop of the IgV domain in the ability of mB7H3 to inhibit naïve T-cell proliferation *in vitro*. Our findings provide insights for the structure-guided design of the next-generation cancer immunotherapeutics.

Results

mB7H3 is produced by Drosophila S2 cells as a glycosylated monomer

B7 family members share low sequence identity but possess a common domain structure (Fig. 1A) and have a similar mode of interaction with receptors belonging to the CD28 protein family. The ectodomain of murine B7-H3 is composed of a single IgV-IgC domain pair (amino acids 34–247) and was produced as a secreted His_6-tagged protein (mB7H3) using Schneider 2 (S2) *Drosophila* cells. Although the predicted molecular weight of mB7H3 was 24 kDa, purified protein behaved as a ~39-kDa species (Fig. 1B) in sodium dodecyl sulfate-polyacrylamide gel electrophoresis (SDS-PAGE), indicating the presence of glycan modifications at some of the four predicted N-linked glycosylation sites (N91, N104, N189, and N215). The presence of glycans was verified by digestion with peptide N-glycosidase F (PNGase F), which resulted in the reduction of the molecular weight of the mB7H3 to ~30 kDa (Fig. 1B). Native protein eluted as a ~40-kDa species in a size-exclusion chromatography (SEC) column (Fig. 1C). Taken together, our data indicate that mB7H3 is expressed as a glycosylated monomer.

Crystal structure of mB7H3

To define the oligomeric organization of mB7H3 and predict its receptor-binding surfaces, we determined its crystal structure (Table 1). The mB7H3 crystals exhibited diffraction consistent with the space group $P6_122$ (a = 100.9 Å, b = 100.9 Å, c = 188.2 Å; one molecule per asymmetric unit), which extended to 2.97 Å. The final refined model accounts for residues 35–151 and 157–239 of mB7H3 with residues 152–156 omitted from the model due to poorly defined electron density, while residues 240–247, although present in the expression construct, were not observed in the electron density.

Pairs of mB7H3 molecules related by crystallographic 2-fold axes form extensive contacts, arising from the mutual exchange of the IgV domains between the neighboring molecules (Fig. 2A). The segment connecting F and G strands (the FG loop) of the IgV domain (residues 135–138) adopted an extended “β-strand-like” conformation—supported by unambiguous electron density (Figs. 2B, S1)—in contrast to the turn-like FG-loop conformation found in the classical IgV domain structures. As a result, the IgV domain of dimeric mB7H3 consists of a β-sandwich composed of a “back-sheet” (BED) and a “front-sheet” (C″C′CFG*), the latter of which includes the G* strand contributed by the second protomer.

The C-terminal IgC domain (residues 140–239) consists of a typical β-sandwich composed of sheets ABED and CFG (Sun and Boyington, 2001). Topologically, this places both IgC domains on the opposite ends of the elongated mB7H3 dimer, with the C-termini separated by ~155 Å.

The mB7H3 sequence contains four potential glycosylation sites: N91, N104, N189, and N215. Electron density that could be interpreted as a single N-acetyl glucosamine (NAG) moiety was present near N91. In the case of N104, three well-ordered sugar residues were observed, corresponding to two NAG and two mannose units. Notably, the location of the glycans on the mB7H3 IgV domain corresponds to the domain's "back-sheet," consistent with the hypothesis that the "front-sheet" engages the receptor, as shown for other B7-family members.

Although the dimer assembly observed in the crystals is stable in solution (see below), mB7H3 was initially purified as a monomer (Fig. 1C), which is likely the dominant form present on the cell surface. To generate a model of the monomeric form of mB7H3, we built a "hybrid" model consisting of residues 35–125 from one protomer and residues 130–238 from its 2-fold symmetry-related mate (Fig. 2C); predicted FG-loop residues (126–129) were modeled as a β-turn using the ArchPRED software (Fernandez-Fuentes et al., 2006). The resulting monomeric mB7H3 model aligns well with a representative B7-family member structure—i.e., human PD-L1 (PDB ID: 3BIK, chain A; overall C_α r.m.s.d. ~2.7 Å, IgV C_α r.m.s.d. ~1.1 Å; Fig. 2D)—indicating that the overall organization of the proposed mB7H3 monomer is consistent with those of other B7-family members.

The FG loop is important for mB7H3-mediated inhibition of T-cell proliferation

Guided by the receptor-binding properties of other immunoglobulin superfamily members and the model of monomeric mB7H3, we generated a panel of mutants targeting the surface residues of the "front-sheet" of the N-terminal IgV domain, including the FG loop (Fig. 3B). This surface has been shown to play a critical role in receptor recognition for a number of B7-family members, including B7-1 (Stamper et al., 2001), B7-2 (Schwartz et al., 2001), PD-L1 (Lin et al., 2008) and PD-L2 (Lázár-Molnár et al., 2008).

B7-H3 function has been previously evaluated in T-cell proliferation assays (Chapoval et al., 2001; Suh et al., 2003; Prasad et al., 2004). In our assay, purified proteins were immobilized on plastic tissue culture plates in the presence of monoclonal anti-murine-CD3 antibody (which was used to engage the TCR-mediated "signal 1"). To ensure a homogeneous T-cell activation state, TCR-transgenic OT-II cells were used in these experiments. $CD4^+$ T cells, freshly isolated from OT-II mice, were incubated in these plates to compare cell proliferation in presence of wild-type or mutant mB7H3 proteins (the optimal mB7H3 concentration was determined, as shown in Fig. 3A). To eliminate possible complications associated with mB7H3 dimers, freshly purified protein stocks were kept at concentrations below 2 mg/mL (details of mB7H3 dimerization are described below).

The presence of wild-type mB7H3 consistently resulted in a ~50% decrease in T-cell proliferation compared to control conditions (PBS or rat IgG), indicating that mB7H3 delivered a signal that was inhibitory to T cells (Fig. 3C). In this assay, the greatest effect was associated with the exchange of the B7-H3 FG-loop sequence with the corresponding sequence from human PD-L1. This chimeric FG-loop mutant (I126Y/Q127G/D128G/F129A) showed a consistent and significant ($p < 0.05$) difference with respect to the wild-type mB7H3, resulting in a nearly complete loss of inhibitory activity (Fig. 3C). In contrast, FG-loop point-mutants I126T and F129A were not significantly different from wild-type

mB7H3. Surprisingly, none of the point-mutants that targeted the “front-sheet” of the mB7H3 IgV domain resulted in a statistically significant change in OT-II T-cell inhibition. Similar data were obtained using $CD4^+$ T cells isolated from C57BL/6 mice (which express a normal T-cell repertoire, in contrast to OT-II cells), with the exception of the T121A mutant, which was significantly impaired in its inhibitory function compared to wild-type mB7H3 (Fig. S2). Taken together, these data show that receptor recognition by B7-H3 involves the residues of the FG loop, but that mutation of individual “front-sheet” residues to alanine is insufficient to disrupt its T-cell inhibitory function.

B7-H3 does not bind TLT-2

The identity of the receptor(s) responsible for the T-cell coinhibitory and costimulatory effects of B7-H3 has not been conclusively established. While expression of the triggering receptor expressed on myeloid cell (TREM)-like transcript-2 (TLT2) has been reported to specifically bind B7-H3 and result in B7-H3-dependent T-cell stimulation (Hashiguchi et al., 2008), these findings could not be reproduced in similar experimental systems using murine or human cells (Leitner et al., 2009). To address these discrepancies, we expressed the ectodomain of murine TLT-2 as a secreted His_6-tagged protein (mTLT2) using S2 cells, and found that mTLT2 and mB7H3 did not bind to each other in SEC or surface plasmon resonance experiments (data not shown). Furthermore, murine B7-H3 Ig-fusion could not bind TLT-2-expressing cells in flow cytometry experiments (data not shown). These observations suggest that TLT-2 is not a binding partner for B7-H3.

mB7H3 forms a stable dimer upon extended incubation at high protein concentration

Stock solutions of purified mB7H3 used in crystallization experiments were routinely concentrated to >10 mg/mL and stored at 4°C. Following extended storage (>3 weeks), we observed a time- and concentration-dependent accumulation of a high-molecular-weight protein species by SEC (Figs. 4A and 4B). This new SEC peak eluted at a volume corresponding to a protein of ~80 kDa—double that of monomeric mB7H3—and did not revert to the original SEC elution profile (corresponding to ~40 kDa) following purification and dilution (data not shown). SDS-PAGE analysis indicated that this protein species was indistinguishable from the original mB7H3 sample, when denatured (Fig. 1B). Furthermore, the complex was found to contain no interchain disulfide bonds when separated under nonreducing conditions (Fig. 1B).

To identify the physicochemical properties responsible for mB7H3 dimer formation, we subjected monomeric mB7H3 to a range of ionic strengths, redox conditions, pHs and temperatures. None of the conditions tested promoted dimer formation (data not shown).

Dimerization of mB7H3 is perturbed by mutations in the FG loop

The four-residue sequence I(Q/R)DF (126–129) of the FG loop in B7-H3 is conserved among the mammalian B7-H3 sequences (Fig. 5A). It is also strikingly different from the corresponding YGGA sequence conserved in the homologous murine PD-L1 (Fig. 5B), the structure of which has been previously reported (PDB ID’s: 3BIK, 3BIS, 3SBW, 3FN3). Based on the fact that in our structure the FG-loop sequence adopts a strand-like conformation, we hypothesized that the it may play a role in mB7H3 dimerization. To assess

this possibility, we monitored the dimerization of mutants I126T, F129A, and the FG-loop chimera (I126Y/Q127G/D128G/F129A) (Fig. 6A).

Each mutant was expressed and purified using the S2 *Drosophila* system described above, and dimer formation was evaluated by SEC, as described for the wild-type mB7H3. Compared to that of wild-type mB7H3, dimer formation was significantly slower for mutants I126T and the FG-loop chimera, whereas mutant F129A exhibited behavior similar to the wild type mB7H3 (Fig. 6B and Table 2).

Both monomeric and dimeric mB7H3 inhibit the proliferation of $CD4^+$ T cells

In order to determine whether dimerization plays a role in mB7H3 function, we compared monomeric mB7H3 to pre-dimerized samples in the T-cell proliferation assay described above. Freshly-purified protein stocks were kept at concentrations below 2 mg/mL to prevent mB7H3 dimerization, and the dimeric samples were verified to be stably dimeric over the course of the experiments (data not shown).

As described above, wild-type monomeric mB7H3 caused a consistent ~50% decrease in T-cell proliferation compared to control conditions (PBS or rat IgG), indicating that mB7H3 delivered an inhibitory signal to the T cells (Fig. 6C: “wt monomer”), whereas the replacement of the FG loop caused near loss of the inhibition (Fig. 6C: “FG chimera”). In order to test the dimeric form of mB7H3, a sample undergoing dimerization and containing ~40% mB7H3 dimer was separated by SEC, and the resulting monomer and dimer fractions were tested (Fig. 6C: samples “wt monomer*” and “wt dimer*”). We found that dimeric mB7H3 did not significantly differ from the monomeric form in its ability to inhibit T-cell proliferation. This indicates that dimerization of mB7H3 alone does not alter the inhibitory property on the molecule.

Discussion

B7-H3 structure

Here we present the structure of the murine B7-H3 ectodomain, which reveals a non-canonical quaternary structure previously described for other members of the Ig superfamily. We observed mB7H3 dimers formed by an unusual strand/domain swap between partner molecules (Fig. 2A), resulting in an elongated assembly with the C-termini separated by ~155 Å. Notably, crystals formed only from protein stocks that had been stored for several weeks following purification, while freshly purified samples failed to yield crystals. Furthermore, we did not identify any crystallization conditions for the FG-loop chimera, which was severely impaired in its capacity to dimerize (Fig. 6B). The dimeric arrangement is stabilized by the exchange of the F strands in the partner molecules within the IgV fold of the N-terminal domain. The sequence connecting the F and G strands, which normally forms the FG loop, is fully extended in the dimer and forms a short two-stranded bridge between the two protomers. This organization is distinct from the typical mode of dimerization in the immunoglobulin superfamily, which involves contacts between two “front-sheets” of the IgV domains from interacting partner molecules (reviewed in Chattopadhyay et al., 2009).

Nevertheless, similar dimers have been described for at least three other members of the immunoglobulin superfamily: the llama antibody VHH-R9 domain (Spinelli et al., 2004), the human CD47 IgV domain (Hatherley et al., 2008), and the CTLA-4 IgV domain (Sonnen et al., 2010) (Fig. 7). According to these reports, dimer formation was not detected in solution, although all of these molecules crystallized as dimers linked by the swap of the G-strand (similar to the mB7H3 structure reported here). In addition, CTLA-4 IgV domain spontaneously forms amyloid aggregates.

In addition to yielding the structure of the dimeric form of mB7H3, our data provided us with a plausible model of its monomeric precursor (Fig. 2C). In particular, the overall superposition of the mB7H3 monomeric model and the human PD-L1 structure (3BIK) demonstrates that the individual IgV- and IgC-domain folds, as well as their positions with respect to one another align well (Fig. 2D). This observation suggests that the invading G strand from each of the protomers occupies a position in the accepting IgV domain of its partner molecule that is equivalent to its position in the monomeric precursor.

B7-H3 function

The precise function of B7-H3 remains unclear, as it has been reported to stimulate (Chapoval et al., 2001; Hashiguchi et al., 2008; Kobori et al., 2010), inhibit (Suh et al., 2003; Prasad et al., 2004; Xu et al., 2006; Leitner et al., 2009; Chen et al., 2011) and have no effect (Steinberger et al., 2004) on T-cell proliferation in various experimental systems. Understanding the role that B7-H3 plays in immunity is further confounded by the fact that B7-H3-deficient mice are generally healthy and have normal cellular compositions of their immune compartments (Suh et al., 2003), suggesting that the loss of B7-H3 function in these animals can be compensated for by other mechanisms. Nevertheless, most reports to date suggest that T cells express an unidentified receptor(s) that binds to B7-H3, resulting in a modulation of the T-cell response to antigen-dependent signals.

In order to study the biological activity of mB7H3, we tested purified protein samples in an *in vitro* system similar to those described earlier (Prasad et al., 2004; Hashiguchi et al., 2008; Suh et al., 2003). Although we initially used C57BL/6-derived T cells, we found that the experimental variation was significantly lower with the cells isolated from OT-II mice. Despite the differences, the data from these two mouse strains was, generally, in agreement. $CD4^+$ T cells isolated from either C57BL/6 or OT-II mice showed a reproducible ~50% inhibition of proliferation when cultured in tissue-culture plates pretreated with a combination of anti-CD3 and wild-type mB7H3, compared to control conditions (anti-CD3 alone or in combination with an irrelevant protein) (Figs. 3C and S2). Thus, in our system we observed that B7-H3 plays an inhibitory role in T-cell activation.

Based on the similar modes of receptor recognition among the B7 family members (Lázár-Molnár et al., 2008; Lin et al., 2008; Stamper et al., 2001; Schwartz et al., 2001), we hypothesized that the residues located on the surface of the “front-sheet” of the IgV domain are involved in recognition of the B7-H3 receptor. A number of mutants on the “front-sheet” surface (I126T, F129A, F123A, I66A, L75A, T121A, Q68A, S78A) had inhibitory activities that could not be distinguished from that of wild-type mB7H3 using the OT-II cells (Fig. 3C) or the C57BL/6-derived cells (with the exception of the T121A mutant, which showed a

significant impairment) (Fig. S2). Taken together our data suggest that either the individual contributions of these residues are insufficiently strong to be detected in our assay or that this molecular surface does not make major contributions to recognition by the receptor.

In contrast, simultaneous multiple mutations resulting from the replacement of the FG loop with the corresponding sequence from murine PD-L1 (FG chimera) resulted in a nearly complete loss of inhibition of OT-II cells (Fig. 3C) and a significant impairment of inhibition of C57BL/6-derived cells (Fig. S2). These data indicate that the FG-loop residues are involved in B7-H3 interaction with the receptor expressed on T cells.

Recombinant B7-H3 dimerization

We demonstrated that mB7H3 spontaneously dimerizes under physiologic pH and ionic strength. This behavior raises questions as to whether the mB7H3 dimer represents a physiologically significant species. In particular, how can the slow kinetics support significant dimer formation*in vivo*? At least three hypotheses emerge: (1) topological restrictions imposed by the association with the plasma membrane of interacting cells may provide a stabilizing environment during monomer/dimer transition under physiologic conditions; (2) additional membrane-associated molecules facilitate the process of mB7H3 dimer formation on the cell surface or in an intracellular compartment; or (3) the crystallographically observed mB7H3 dimer may be an *in vitro* artifact with no *in vivo* correlate.

Based on the comparison between the model of the mB7H3 monomer and the observed dimer structure, we hypothesized that the sequence connecting the strands F and G of the IgV domain can adopt at least two conformations (extended and β-turn-like) and thus plays a role in the ability of B7-H3 to dimerize. To address this hypothesis, we generated a series of mutants targeting the loop connecting the F and G strands. Introduction of the FG-loop sequence (YGGA) from PD-L1, containing the highly flexible Gly-Gly pair of residues, severely impaired dimer formation with an ~18-fold reduction in the rate of dimerization.

Additionally, when modeled in the β-turn conformation (i.e., in the monomeric form), the predicted geometry of the mB7H3 FG loop would cause the hydrophobic residue Ile-126 to be more solvent-exposed than in the extended conformation observed in dimeric mB7H3. In the latter case, the Ile-126 side chain interacts more tightly with the hydrophobic side chains of Phe-52 and Phe-58, stabilizing the extended conformation of the mB7H3 protomer and the dimer itself. Introduction of the I126T mutation in mB7H3 resulted in a ~3-fold reduction in the dimerization rate, supporting the hypothesis that hydrophobicity of Ile-126 contributes to dimer formation. Taken together, our analysis of the FG loop in mB7H3 suggests that the wild-type sequence may play a destabilizing role for the monomeric form of mB7H3.

Implications B7-H3 dimerization for biological function

The functional relevance of strand-swapped dimer formation among the Ig superfamily members is not clear. Of the known examples, strand exchange of the llama antibody VHH domain would render it incapable of engaging antigen due to the remodeling at the antigen-

binding site. In CD47, the N-terminal IgV domain is topologically constrained with respect to the C-terminal portions of the molecule, making it unlikely to participate in the strand-swap dimerization while expressed on the cell surface. On the other hand, amyloid fiber formation by CTLA-4 suggests a potential mechanism by which strand-swapping may lead to a variety of diseases associated with immunoglobulin deposition (Bennett et al., 2006). Although B7-H3 has not been implicated in amyloid-caused disease, our data lend credence to the notion that IgV domains may exhibit unanticipated plasticity.

The B7-H3 dimer structure reported here positions the transmembrane regions of the molecule at a ~155-Å distance. This arrangement is suggestive of a mechanism by which homophilic B7-H3 interactions may bridge two interacting cells and may possibly represent a ligand:ligand or a ligand:receptor complex (in which case one or both of the B7-H3 molecules would facilitate signalling to its parent cell). Interestingly, our structure predicts that if the “front-sheet” of the B7-H3 IgV domain is involved in receptor recognition, the binding surface would be accessible in the dimeric form of B7-H3. Furthermore, in our experiments the mB7H3 dimer had the same inhibitory activity as the monomer in the T-cell proliferation assay (Fig. 6C), which is consistent with this notion. However, due to the slow rate of mB7H3 dimer formation measured in solution (Table 2) it is likely that additional mechanisms are involved in facilitating B7-H3 dimerization, if it plays a role in B7-H3 function.

Finally, we have shown that the inhibitory activity of mB7H3 FG chimera is severely impaired and that this mutant is also impaired in its ability to dimerize in solution. Although these observations are intriguing, we believe that they are unlikely to be related for the following reasons: (1) the monomeric and dimeric forms of mB7H3 are functionally equivalent in our T-cell proliferation assays (Fig. 6C) and (2) the I126T mutant is functional in the T-cell proliferation assays (Figs. 6C and S2) but is significantly impaired in its dimerization properties (Fig. 6B). Thus, our data lead us to conclude that whereas both conformations of the FG loop are equally functional, the identities of the residues of the FG loop are critical for receptor recognition.

In summary, we determined the structure of murine B7-H3 and used it to characterize the molecular determinants responsible for receptor recognition. A growing body of literature suggests that B7-H3 is a key factor in the progression of many cancers and highlights the importance of studies of the biology of this molecule as well as its binding partners, which control the immune response at tumor sites. Although the precise role that B7-H3 plays in *in vivo* T-cell regulation remains to be defined, we demonstrated that it has a clear inhibitory function in our assay system and identified the FG-loop sequence in its IgV domain as important for this function. The development of therapeutics specifically targeting this sequence may prove useful as an anticancer drug strategy.

Experimental Procedures

DNA cloning

DNA encoding the predicted extracellular fragment of murine B7-H3 (amino acids 34–247) was amplified by PCR using primers containing BglII and AgeI restriction sites and cloned

into the pMT/BiP/V5-His A (Invitrogen) or the pCGMbX vector, which includes a constitutively expressed *egfp* gene. Constructs containing mutations of single residues and contiguous spans were generated using Quickchange site-directed mutagenesis (Stratagene).

Cell Lines

Express Five SFM serum-free medium (Invitrogen) was used for routine culture and recombinant protein expression using *Drosophila*S2 cells. Schneider's *Drosophila* Medium (Invitrogen), supplemented with 10% fetal bovine serum, was used when transfecting the cells using the calcium phosphate method (Invitrogen). Alternatively, transfection was performed using the dimethyl dioctadecyl ammonium bromide (DDAB) method (Han, 1996) in Express Five SFM. Following cotransfection of the target-containing vector and the selection vector (pCoBlast or pCoPuro; mixed at a ratio of 1:20 with the target-containing vector), the cells were allowed to recover for ~48 hours before being selected with either 25 μg/mL Blasticidin S (Invitrogen) or 10 μg/mL puromycin (Fisher). To improve protein expression, drug-resistant cell populations were subcloned using a modified version of the limited dilution method (Yang et al., 2004). Briefly, parental S2 feeder cells were irradiated (20,000 rads) and co-plated with target stable cell populations at a ratio of 250,000:3 (feeder : target) per well of a 96-well plate. The target cells were allowed to form colonies over the course of 2–3 weeks while being supplemented with fresh medium every 4–6 days. The colonies were then resuspended and replica-plated into an induction plate containing fresh medium supplemented with 1 mM copper sulfate. Following a 7-day incubation, the supernatants from the induction plate were screened by dot-blot using Penta-His antibody (Qiagen) to identify the high-expressors among the stable cell line populations.

Animals

C57BL/6 and OT-II mice were purchased from The Jackson Laboratory (Bar Harbor, ME), and maintained under pathogen-free conditions at the Albert Einstein College of Medicine. OT-II mice carry an MHC class-II-restricted chicken ovalbumin-specific TCR transgene, thus narrowing the specificity of their entire T-cell repertoire to just this antigen. Mice were used in the experiments at 6–12 weeks of age. All animal work was performed according to the guidelines set by the Institutional Animal Care and Use Committee.

Protein Expression and Purification

Cell lines were expanded in shaker-flask suspension cultures and induced with 1 mM copper sulfate. Cultures were harvested 7 days post-induction, centrifuged to remove cells and debris, supplemented with 150 mM NaCl and 0.02% sodium azide, and filtered using 0.22-μm membrane. The resulting clarified supernatants were flowed over a column containing Ni-NTA agarose (Qiagen), washed with TBS (20 mM Tris-HCl, pH 8; 300 mM NaCl; 0.02% sodium azide), TBS + 20 mM imidazole, and eluted using TBS + 200 mM imidazole. Eluted protein was concentrated and further purified using gel filtration on Superdex-200 resin in HBS-E buffer (20 mM Hepes, pH 7; 150 mM NaCl; 1 mM EDTA).

Crystallization, Data Collection, and Modeling

Diffraction-quality crystals were grown in sitting-drop crystallization reactions containing 1 μL of protein solution (10 mg/mL in HBS-E) and 1 μL reservoir solution (0.1 M Hepes, pH 7.5 and 20% polyethylene glycol 10,000 [w/vol]). Crystals were cryo-protected in reservoir solution supplemented with 20% ethylene glycol (vol/vol) prior to flash-cooling in liquid nitrogen. X-ray diffraction data were collected at beamlines 24-ID-E (Advanced Photon Source, Argonne, IL) and X29 (National Synchrotron Light Source, Upton, NY).

Data were integrated using the iMosflm (Battye et al., 2011) software with subsequent processing using the programs within the CCP4 software package (Winn et al., 2011). An initial structure, based on the structure of human PD-L1 (PDB ID: 3BIK), was determined using the BALBES software package (Long et al., 2008). The model was further built using Coot (Emsley et al., 2010) and refined using REFMAC5 (Murshudov et al., 1997). The structure factors and the final model have been deposited into the Protein Data Bank and have been assigned the PDB ID 4I0K.

Dimerization Kinetics Measurements

Concentrated wild-type and mutant mB7H3 protein stocks were serially diluted in HBS-E buffer and incubated at 4°C. Aliquots containing ~50 μg of protein were separated on a standardized analytical Superdex-200 sizing column and the peak heights (absorbance at 280 nm) corresponding to monomer and dimer protein species were recorded for the duration of each time course. Concentrations of monomer and dimer species were estimated based on the fraction of peak heights of each component with respect to total protein amount. These data were used to generate a global fit (using data from multiple concentrations of each protein) against a model for a second-order reaction rate law (as shown in Fig. S3) using GraphPad Prism (ver. 5) software to obtain the apparent association rate constants shown in Table 2.

T-cell Proliferation Assays

$CD4^+$ T cells were isolated from the spleens and superficial lymph nodes of 6–8 weeks old OT-II or C57BL/6 mice, using mouse CD4 Dynabeads and DETACHaBEADs (Invitrogen). 2×10^5 purified $CD4^+$ T cells were plated into each well of a 96-well cell culture plate precoated (for 16 hours at 4°C) with 0.5-μg/mL solution of CD3ε antibody (BD Biosciences), also containing the indicated amounts of either wild-type mB7H3 monomer, mB7H3 dimer, mB7H3 mutants, rat IgG2b (Bio Express), as a protein control, or a PBS control. [^{3}H]-thymidine (Perkin Elmer) was added for the last 18 hours of the 72-h cultures, and T-cell proliferation was measured by detecting ^{3}H-incorporation using a Wallac Microbeta 1450 Trilux liquid scintillation counter. Where indicated, data were normalized with respect to the average signal obtained with anti-CD3/PBS control. Replicates of at least four wells were used for each condition, and the experiments were repeated 2–5 times. Optimal concentrations of anti-CD3 and monomeric mB7H3—specific to our assay system—were determined by dose-response titration experiments such as the one shown in Fig. 3A. The data were analyzed using one-way ANOVA followed by Dunnett's multiple comparison test (GraphPad Prism, ver. 5), p values < 0.05 were considered significant.

Supplementary Material

Refer to Web version on PubMed Central for supplementary material.

Acknowledgments

The authors gratefully acknowledge Dr. Jeffrey B. Bonanno for helpful discussions during structure determination, Dr. Kaya Ghosh for her contributions to the T-cell-based assay setup, Dr. Deborah Palliser for her help with the experimental design and Dr. Teresa P. DiLorenzo for her insightful suggestions during the writing of this manuscript. This work was supported in part by NIH grants GM094662 (SCA), GM094665 (SGN), AI007289 (SGN and SCA), DP2DK083076 (XZ), CA009173 and the Irvington Institute Fellowship Program of the Cancer Research Institute (VV), and Department of Defense Grant PC094137 (XZ). The Albert Einstein Cancer Center is supported by NIH P30CA013330.

References

Barach YS, Lee JS, Zang X. T cell coinhibition in prostate cancer: new immune evasion pathways and emerging therapeutics. Trends in Molecular Medicine. 2010; 17:47–55.

Battye TGG, Kontogiannis L, Johnson O, Powell HR, Leslie AGW. iMOSFLM: a new graphical interface for diffraction-image processing with MOSFLM. Acta Crystallogr D Biol Crystallogr. 2011; 67:271–281. [PubMed: 21460445]

Bennett MJ, Sawaya MR, Eisenberg D. Deposition diseases and 3D domain swapping. Structure. 2006; 14:811–824. [PubMed: 16698543]

Chapoval AI, Ni J, Lau JS, Wilcox RA, Flies DB, Liu D, Dong H, Sica GL, Zhu G, Tamada K, et al. B7-H3: a costimulatory molecule for T cell activation and IFN-gamma production. Nat Immunol. 2001; 2:269–274. [PubMed: 11224528]

Chattopadhyay K, Lázár-Molnár E, Yan Q, Rubinstein R, Zhan C, Vigdorovich V, Ramagopal UA, Bonanno J, Nathenson SG, Almo SC. Sequence, structure, function, immunity: structural genomics of costimulation. Immunol Rev. 2009; 229:356–386. [PubMed: 19426233]

Chen W, Hou Z, Li C, Xiong S, Liu H. Cloning and characterization of porcine 4Ig-B7-H3: a potent inhibitor of porcine T-cell activation. PLoS ONE. 2011; 6:e21341. [PubMed: 21738638]

Crispen PL, Sheinin Y, Roth TJ, Lohse CM, Kuntz SM, Frigola X, Thompson RH, Boorjian SA, Dong H, Leibovich BC, et al. Tumor cell and tumor vasculature expression of B7-H3 predict survival in clear cell renal cell carcinoma. Clin Cancer Res. 2008; 14:5150–5157. [PubMed: 18694993]

Emsley P, Lohkamp B, Scott WG, Cowtan K. Features and development of Coot. Acta Crystallogr D Biol Crystallogr. 2010; 66:486–501. [PubMed: 20383002]

Fernandez-Fuentes N, Zhai J, Fiser A. ArchPRED: a template based loop structure prediction server. Nucleic Acids Res. 2006; 34:W173–176. [PubMed: 16844985]

Gouet P, Courcelle E, Stuart DI, Métoz F. ESPript: analysis of multiple sequence alignments in PostScript. Bioinformatics. 1999; 15:305–308. [PubMed: 10320398]

Goujon M, McWilliam H, Li W, Valentin F, Squizzato S, Paern J, Lopez R. A new bioinformatics analysis tools framework at EMBL-EBI. Nucleic Acids Res. 2010; 38:W695–699. [PubMed: 20439314]

Han K. An efficient DDAB-mediated transfection of Drosophila S2 cells. Nucleic Acids Res. 1996; 24:4362–4363. [PubMed: 8932397]

Hansen JD, Du Pasquier L, Lefranc MP, Lopez V, Benmansour A, Boudinot P. The B7 family of immunoregulatory receptors: a comparative and evolutionary perspective. Mol Immunol. 2009; 46:457–472. [PubMed: 19081138]

Hashiguchi M, Kobori H, Ritprajak P, Kamimura Y, Kozono H, Azuma M. Triggering receptor expressed on myeloid cell-like transcript 2 (TLT-2) is a counter-receptor for B7-H3 and enhances T cell responses. Proc Natl Acad Sci USA. 2008; 105:10495–10500. [PubMed: 18650384]

Hatherley D, Graham SC, Turner J, Harlos K, Stuart DI, Barclay AN. Paired receptor specificity explained by structures of signal regulatory proteins alone and complexed with CD47. Mol Cell. 2008; 31:266–277. [PubMed: 18657508]

Kobori H, Hashiguchi M, Piao J, Kato M, Ritprajak P, Azuma M. Enhancement of effector CD8+ T-cell function by tumour-associated B7-H3 and modulation of its counter-receptor triggering receptor expressed on myeloid cell-like transcript 2 at tumour sites. Immunology. 2010; 130:363–373. [PubMed: 20141543]

Larkin MA, Blackshields G, Brown NP, Chenna R, McGettigan PA, McWilliam H, Valentin F, Wallace IM, Wilm A, Lopez R, et al. Clustal W and Clustal X version 2.0. Bioinformatics. 2007; 23:2947–2948. [PubMed: 17846036]

Lázár-Molnár E, Yan Q, Cao E, Ramagopal U, Nathenson SG, Almo SC. Crystal structure of the complex between programmed death-1 (PD-1) and its ligand PD-L2. Proc Natl Acad Sci USA. 2008; 105:10483–10488. [PubMed: 18641123]

Leitner J, Klauser C, Pickl WF, Stöckl J, Majdic O, Bardet AF, Kreil DP, Dong C, Yamazaki T, Zlabinger G, et al. B7-H3 is a potent inhibitor of human T-cell activation: No evidence for B7-H3 and TREML2 interaction. Eur J Immunol. 2009; 39:1754–1764. [PubMed: 19544488]

Lin DYW, Tanaka Y, Iwasaki M, Gittis AG, Su HP, Mikami B, Okazaki T, Honjo T, Minato N, Garboczi DN. The PD-1/PD-L1 complex resembles the antigen-binding Fv domains of antibodies and T cell receptors. Proc Natl Acad Sci USA. 2008; 105:3011–3016. [PubMed: 18287011]

Ling V, Wu PW, Spaulding V, Kieleczawa J, Luxenberg D, Carreno BM, Collins M. Duplication of primate and rodent B7-H3 immunoglobulin V- and C-like domains: divergent history of functional redundancy and exon loss. Genomics. 2003; 82:365–377. [PubMed: 12906861]

Long F, Vagin AA, Young P, Murshudov GN. BALBES: a molecular-replacement pipeline. Acta Crystallogr D Biol Crystallogr. 2008; 64:125–132. [PubMed: 18094476]

Loos M, Hedderich DM, Friess H, Kleeff J. B7-h3 and its role in antitumor immunity. Clin Dev Immunol. 2010; 2010:683875. [PubMed: 21127709]

Murshudov GN, Vagin AA, Dodson EJ. Refinement of macromolecular structures by the maximum-likelihood method. Acta Crystallogr D Biol Crystallogr. 1997; 53:240–255. [PubMed: 15299926]

Prasad DVR, Nguyen T, Li Z, Yang Y, Duong J, Wang Y, Dong C. Murine B7-H3 is a negative regulator of T cells. J Immunol. 2004; 173:2500–2506. [PubMed: 15294965]

Roth TJ, Sheinin Y, Lohse CM, Kuntz SM, Frigola X, Inman BA, Krambeck AE, McKenney ME, Karnes RJ, Blute ML, et al. B7-H3 ligand expression by prostate cancer: a novel marker of prognosis and potential target for therapy. Cancer Res. 2007; 67:7893–7900. [PubMed: 17686830]

Schwartz JC, Zhang X, Fedorov AA, Nathenson SG, Almo SC. Structural basis for co-stimulation by the human CTLA-4/B7-2 complex. Nature. 2001; 410:604–608. [PubMed: 11279501]

Sharpe AH, Freeman GJ. The B7-CD28 superfamily. Nat Rev Immunol. 2002; 2:116–126. [PubMed: 11910893]

Sonnen AFP, Yu C, Evans EJ, Stuart DI, Davis SJ, Gilbert RJC. Domain metastability: a molecular basis for immunoglobulin deposition? J Mol Biol. 2010; 399:207–213. [PubMed: 20394753]

Spinelli S, Desmyter A, Frenken L, Verrips T, Tegoni M, Cambillau C. Domain swapping of a llama VHH domain builds a crystal-wide beta-sheet structure. FEBS Lett. 2004; 564:35–40. [PubMed: 15094039]

Stamper CC, Zhang Y, Tobin JF, Erbe DV, Ikemizu S, Davis SJ, Stahl ML, Seehra J, Somers WS, Mosyak L. Crystal structure of the B7-1/CTLA-4 complex that inhibits human immune responses. Nature. 2001; 410:608–611. [PubMed: 11279502]

Steinberger P, Majdic O, Derdak SV, Pfistershammer K, Kirchberger S, Klauser C, Zlabinger G, Pickl WF, Stöckl J, Knapp W. Molecular characterization of human 4Ig-B7-H3, a member of the B7 family with four Ig-like domains. J Immunol. 2004; 172:2352–2359. [PubMed: 14764704]

Suh WK, Gajewska BU, Okada H, Gronski MA, Bertram EM, Dawicki W, Duncan GS, Bukczynski J, Plyte S, Elia A, et al. The B7 family member B7-H3 preferentially down-regulates T helper type 1-mediated immune responses. Nat Immunol. 2003; 4:899–906. [PubMed: 12925852]

Sun M, Richards S, Prasad DVR, Mai XM, Rudensky A, Dong C. Characterization of mouse and human B7-H3 genes. J Immunol. 2002; 168:6294–6297. [PubMed: 12055244]

Sun PD, Boyington JC. Overview of protein folds in the immune system. Curr Protoc Immunol. 2001 Appendix 1, Appendix 1N.

Sun X, Vale M, Leung E, Kanwar JR, Gupta R, Krissansen GW. Mouse B7-H3 induces antitumor immunity. Gene Ther. 2003; 10:1728–1734. [PubMed: 12939639]

Winn MD, Ballard CC, Cowtan KD, Dodson EJ, Emsley P, Evans PR, Keegan RM, Krissinel EB, Leslie AGW, McCoy A, et al. Overview of the CCP4 suite and current developments. Acta Crystallogr D Biol Crystallogr. 2011; 67:235–242. [PubMed: 21460441]

Xu J, Huang B, Xiong P, Feng W, Xu Y, Fang M, Zheng F, Gong F. Soluble mouse B7-H3 down-regulates dendritic cell stimulatory capacity to allogenic T cell proliferation and production of IL-2 and IFN-gamma. Cell Mol Immunol. 2006; 3:235–240. [PubMed: 16893505]

Yamato I, Sho M, Nomi T, Akahori T, Shimada K, Hotta K, Kanehiro H, Konishi N, Yagita H, Nakajima Y. Clinical importance of B7-H3 expression in human pancreatic cancer. Br J Cancer. 2009; 101:1709–1716. [PubMed: 19844235]

Yang J, Jaramillo A, Shi R, Kwok WW, Mohanakumar T. In vivo biotinylation of the major histocompatibility complex (MHC) class II/peptide complex by coexpression of BirA enzyme for the generation of MHC class II/tetramers. Hum Immunol. 2004; 65:692–699. [PubMed: 15301857]

Zang X, Sullivan PS, Soslow RA, Waitz R, Reuter VE, Wilton A, Thaler HT, Arul M, Slovin SF, Wei J, et al. Tumor associated endothelial expression of B7-H3 predicts survival in ovarian carcinomas. Mod Pathol. 2010; 23:1104–1112. [PubMed: 20495537]

Zang X, Thompson RH, Al-Ahmadie HA, Serio AM, Reuter VE, Eastham JA, Scardino PT, Sharma P, Allison JP. B7-H3 and B7x are highly expressed in human prostate cancer and associated with disease spread and poor outcome. Proc Natl Acad Sci USA. 2007; 104:19458–19463. [PubMed: 18042703]

Highlights

- Murine B7-H3 ectodomain crystals contain a strand-swapped dimer.
- Recombinant B7-H3 ectodomain inhibits T-cell proliferation.
- Loop sequence mutations in the IgV domain disrupt B7-H3 dimerization and function.

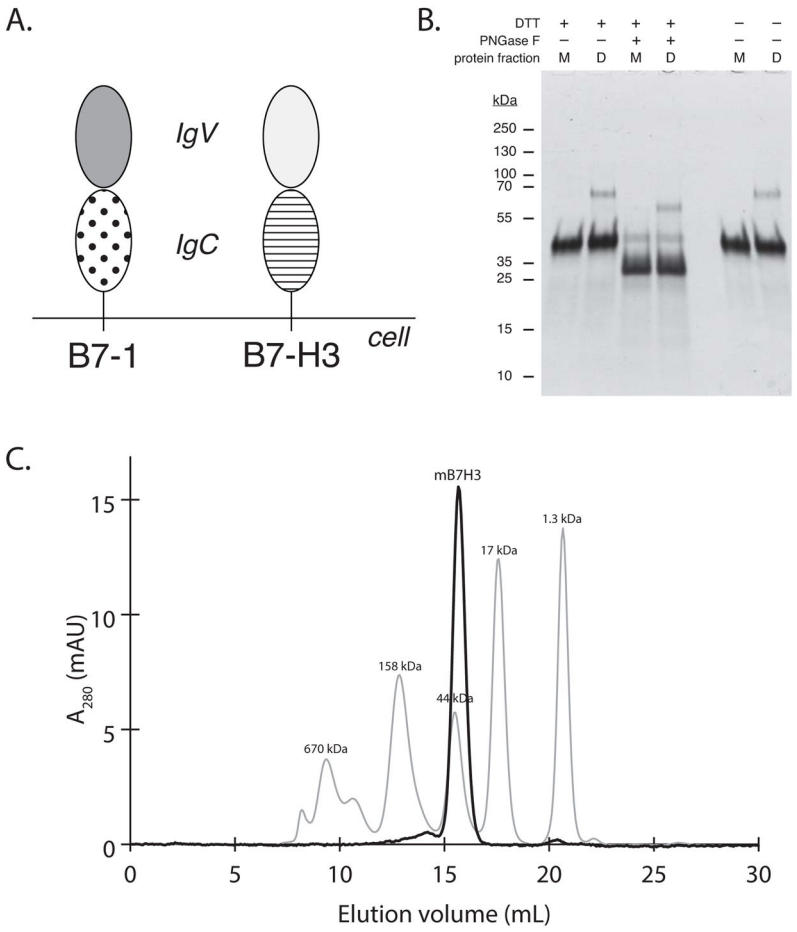

Figure 1. Expression and purification of mB7H3

(A) **Domain organization of murine B7 family members.** Diagrams of murine B7-1 and B7-H3 are shown as the representative members of the B7 family. Molecules are expressed as type-I transmembrane proteins, consisting of an N-terminal IgV and a C-terminal IgC domains, followed by a single transmembrane sequence and a short cytoplasmic tail.

(B) **Purified mB7H3 monomer and dimer species are glycosylated and do not contain interchain disulfide bonds.** SDS-PAGE of purified monomer (M) and dimer (D) forms of mB7H3 were separated in presence or absence of dithiothreitol, and before and after treatment with PNGase F, as indicated above the lanes.

(C) **Native mB7H3 expressed by*Drosophila* S2 cells behaves as a monomer in size-exclusion chromatography.** Purified protein elutes as a monodisperse peak of ~40 kDa on a calibrated Superdex-200 size-exclusion column (dark trace). Molecular weight standards are shown (light trace).

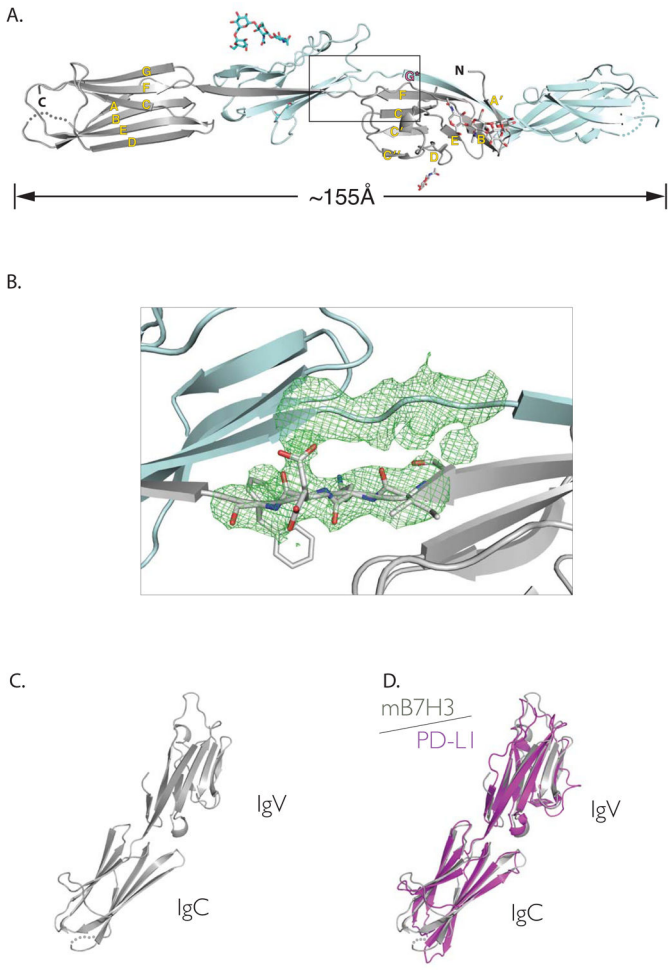

Figure 2. Structure of mB7H3

(A) **Crystals of mB7H3 contain the dimeric form of the protein.** Ribbon representation of the crystallographic dimer of mB7H3 with each protomer drawn in different colors (gray and cyan) with N and C-termini labeled for one of the protomers. Unmodeled residues 152–156 of the IgC domain of each protomer are shown with dots of corresponding color. The glycans (2 on each protomer) are drawn in stick representation. Strands making up the immunoglobulin fold in each domain are labeled in yellow, while the strand exchanged between the two protomers (G*) is labeled in pink.

(B) **Electron density of the extended FG-loop bridging sequence.** *Fo−Fc* electron density map, calculated with the FG-loop sequence omitted, contoured at +3σ is shown in green near the location of the strand exchange highlighted by a box in Fig. 2A. Ribbon diagrams representing the structure for each mB7H3 protomer are shown. The sidechains of the FG-loop residues are shown in gray stick-figure representation. See also Fig. S1.

(C) **Structure-based model of monomeric mB7H3.** Model of the mB7H3 monomer was constructed by combining residues 35–125 from one protomer and residues 130–238 from its 2-fold-related symmetry mate.

(D) **Monomeric model ofmB 7H3 corresponds well to the PD-L1 structure.** Structural alignment (overall C_α r.m.s.d. ~2.7 Å) of the monomeric mB7H3 model (gray) and the structure of human PD-L1 (purple).

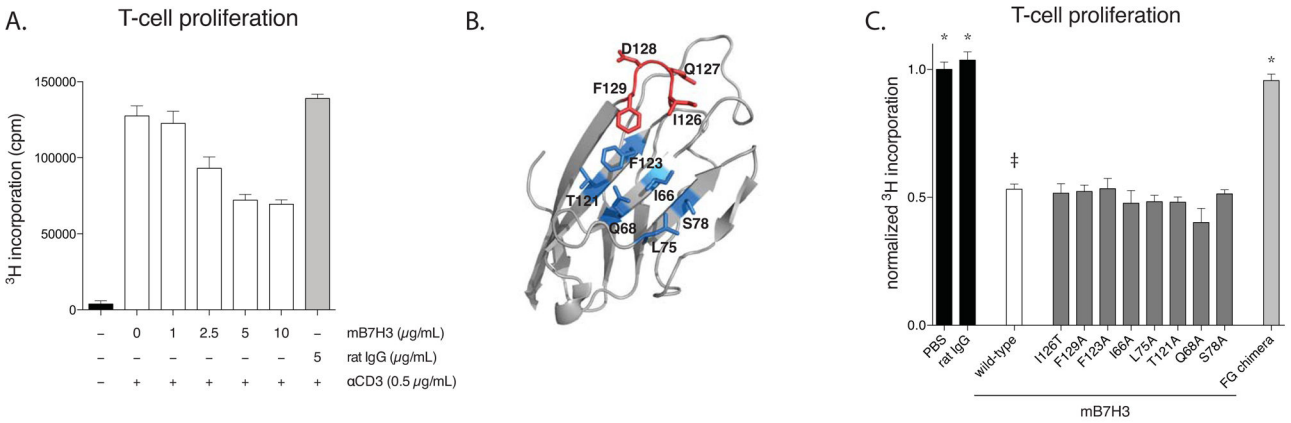

Figure 3. Functional characterization of mB7H3 wild-type and mutants

(A) **CD4$^+$ T-cell proliferation is inhibited by monomeric and dimeric mB7H3 in a dose-dependent manner.** CD4$^+$OT-II cells were cultured in plasticware pretreated with the proteins indicated below the x-axis. T-cell proliferation was assayed by pulsing with [^{3}H]-thymidine during the last 18 hours of a 3-day incubation. Average values obtained from 4 replicates are shown with error bars representing the standard error of mean.

(B) **Mapping of "front-sheet" and FG-loop mutations on the structure of mB7H3.** The N-terminal IgV domain of mB7H3 monomer is shown in ribbon diagram (gray). Residues of the FG loop (red) and mutated "front-sheet" positions (blue) are labeled and shown with sidechains represented as stick figure.

(C) **T-cell proliferation is inhibited by wild-type, but not the FG-loop chimera of mB7H3.** CD4$^+$OT-II T cells were cultured in 96-well plates precoated with 0.5 μg/mL anti-CD3 and 5 μg/mL proteins indicated along the x-axis. T-cell proliferation was assayed by pulsing with [^{3}H]-thymidine during the last 18 hours of a 3-day incubation. Data were normalized to the mean value obtained for anti-CD3 alone (PBS). Average values obtained from 2 experiments (4 replicates per sample per experiment) are shown with error bars representing the standard error of mean. Statistically significant differences ($p < 0.05$, ANOVA) with respect to the wild-type mB7H3 sample (double dagger) are labeled with asterisks. See also Fig. S2.

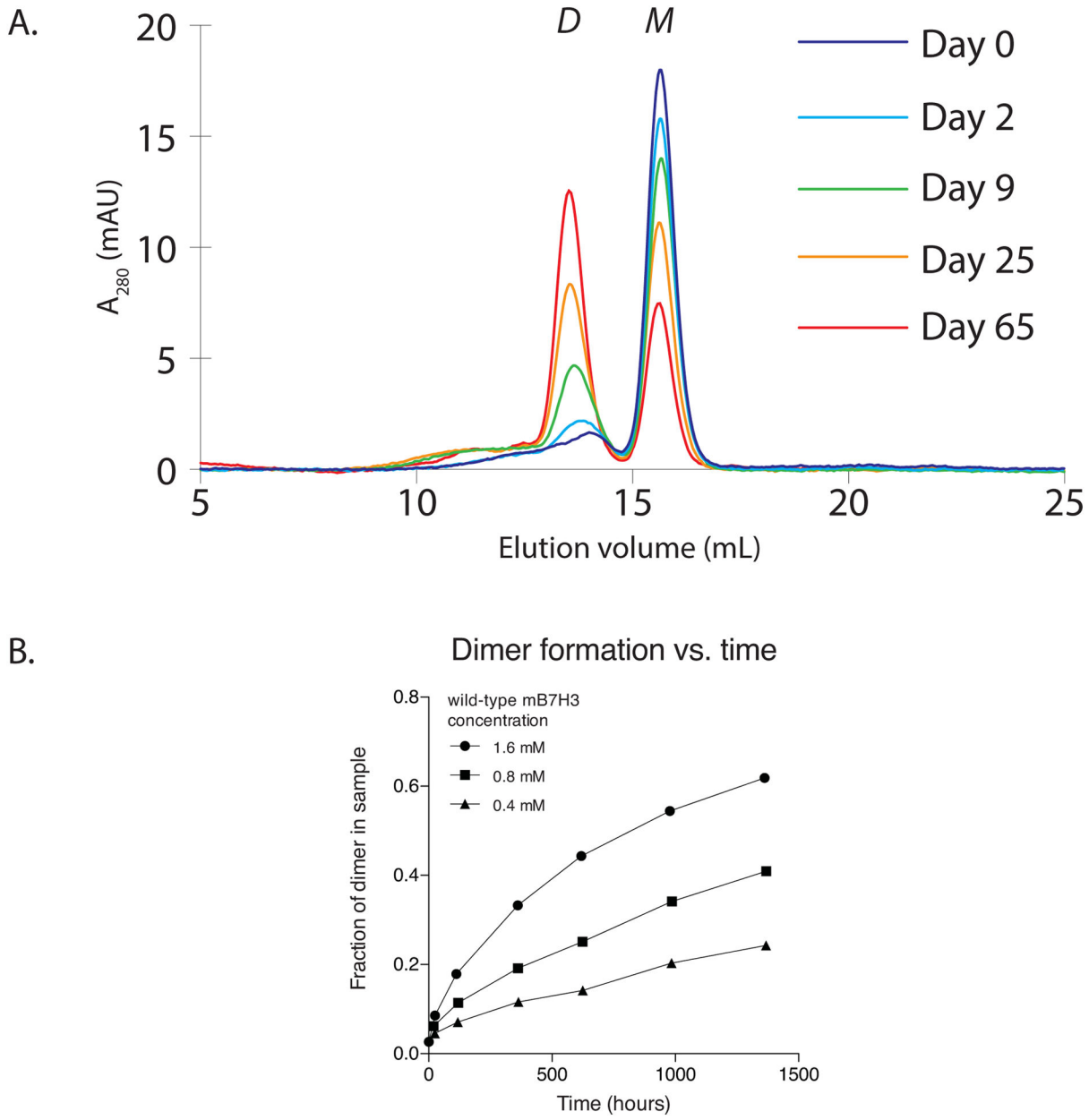

Figure 4. mB7H3 forms stable dimers in solution

(A) **Purified mB7H3 dimerizes during incubation.** Protein samples were concentrated to ~1.6 mM (60 mg/mL) and incubated at 4°C. SEC traces represent experiments carried out at the timepoints indicated. Monomer (M) and dimer (D) peaks are labeled. (B) **Wild-type mB7H3 dimerizes over time in a concentration-dependent manner.** SEC timecourse data similar to those shown in (A) were obtained for the indicated concentrations of wild-type mB7H3. Each data point represents the proportion of dimer observed (as measured by dimer peak height) compared to the total (monomer peak height + dimer peak height).

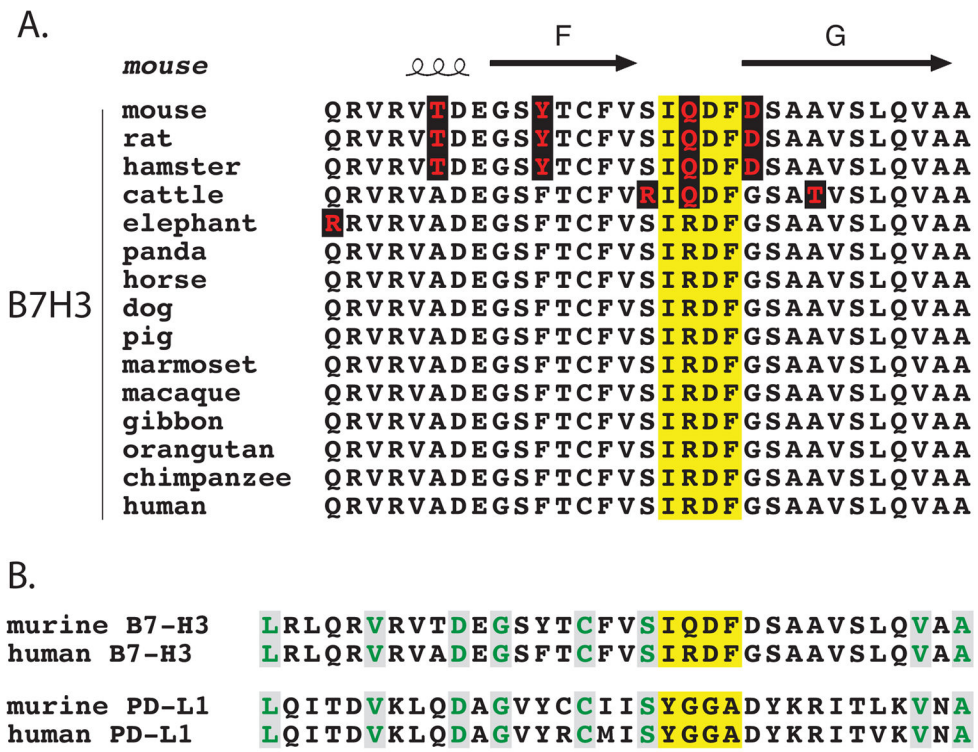

Figure 5. Sequence conservation of the FG loop

(A) **Sequence of the B7-H3 FG loop is conserved.** ClustalW (Larkin et al., 2007; Goujon et al., 2010) was used to align the mB7H3 sequences from 8 mammalian species and the resulting alignment is presented using ESPript (Gouet et al., 1999). Secondary structural elements of the mB7H3 structure are labeled (top line). Sequence differences are shown as red lettering on black background. The 4 FG-loop residues are highlighed with yellow background.

(B) **Sequence of the FG loop is divergent between B7 family members.** ClustalW (Larkin et al., 2007; Goujon et al., 2010) sequence alignment of murine and human sequences of B7-H3 and PD-L1 is shown. Positions identical in all sequences are shown in green lettering with gray background. The 4 FG-loop residues are highlighted with yellow background.

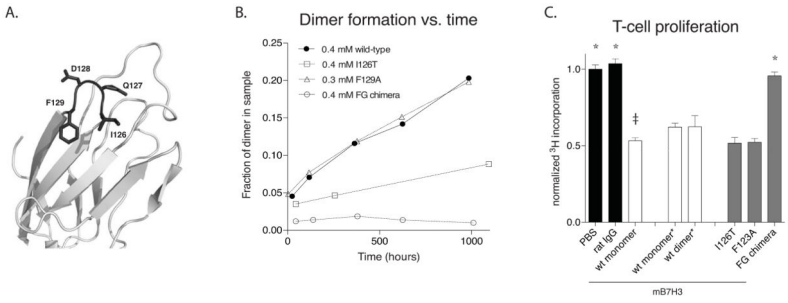

Figure 6. Functional characterization of mB7H3 monomer and dimer

(A) **Mapping FG-loop mutations on the structure of mB7H3.** The N-terminal IgV domain of mB7H3 monomer is shown in ribbon diagram (gray). Residues of the FG loop (black) are labeled and shown with sidechains represented as stick figure.

(B) **Mutations at the FG loop disrupt dimerization of mB7H3.** Dimer formation was measured for mB7H3 FG-loop mutants using experiments similar to those shown in Fig. 4A.

(C) **T-cell proliferation is inhibited by wild-type, but not the FG-loop chimera of mB7H3.** $CD4^+$OT -II cells were cultured in 96-well plates precoated with 0.5 μg/mL anti-CD3 and 5 μg/mL of the proteins indicated along the x-axis. T-cell proliferation was assayed by pulsing with [^{3}H]-thymidine during the last 18 hours of a 3-day incubation. Data were normalized to the mean value obtained for the treatment with anti-CD3 alone (PBS). Average values obtained from 2 experiments (4 replicates per sample per experiment) are shown with error bars representing the standard error of mean. Statistically significant differences ($p < 0.05$, ANOVA) with respect to the wild-type mB7H3 sample (double dagger) are labeled with asterisks.

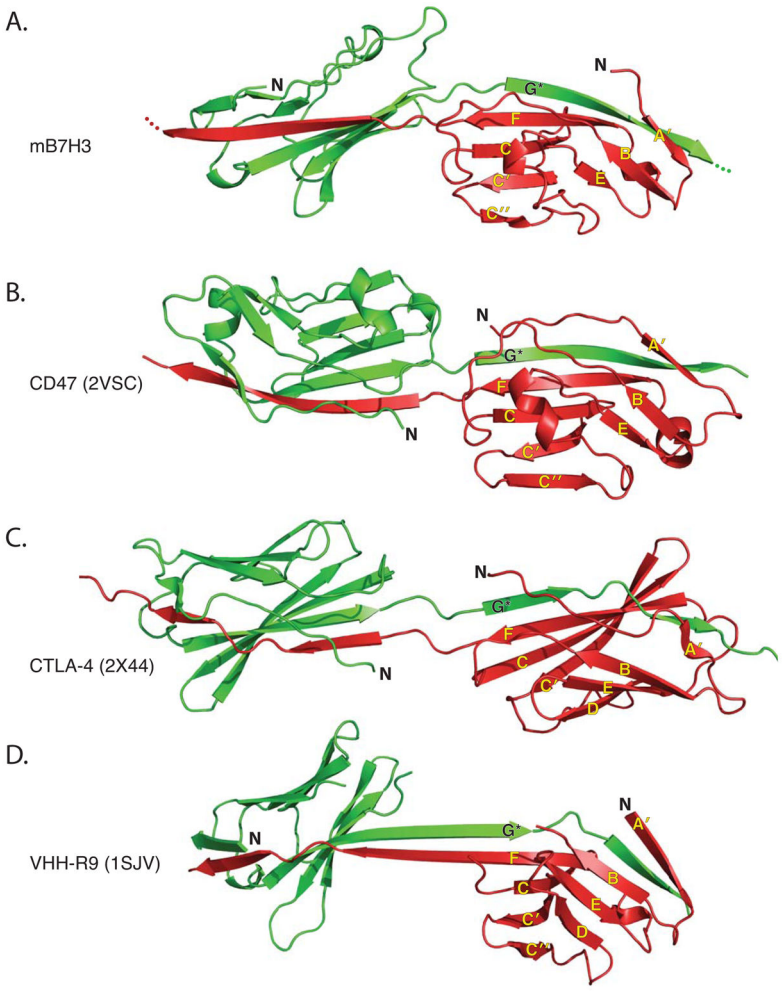

Figure 7. Strand-swapped dimer formation among the members of the immunoglobulin superfamily

Structures of strand-swapped dimers of IgV domains. N-terminal IgV domain dimer of mB7H3 (A), CD47 (B), CTLA-4 (C) and llama VHH-R9 immunoglobulin (D). Each protomer is labeled in different colors (green and red), with N- termini labeled. Strands making up the the two β-sheets of the immunoglobulin fold are labeled (yellow) and the swapped strand (G*) is labeled in black.

Table 1

Crystallographic statistics

Data Collection	
Space group	**P 6_122**
Unit cell:	
a, b, c (Å)	100.9, 100.9, 188.2
α, β, γ (°)	90, 90, 120
Wavelength (Å)	0.9789
Resolution (Å)	50.96–2.97
R_{merge} (%)[a]	11.7 (80.0)
I/σ (I)[a]	18.1 (3.9)
Completeness (%)[a]	99.7 (100.0)
Redundancy[a]	13.1 (13.7)
Refinement	
Number of reflections	11661
R_{work} (%)	21.6
R_{free} (%)	25.0
Number of atoms	
Protein	1526
Water	5
B factors (Å^2)	
Protein	72.28
Water	59.03
Rmsd from ideal geometry	
Bond lengths (Å)	0.012
Bond angles (°)	1.7

[a]The highest-resolution shell is shown in parentheses.

$R_{merge} = \Sigma\ |I - < I >|/\Sigma I$ where I is the integrated intensity of a given reflection.

$R_{work} = \Sigma||F_{obs}| - |F_{calc}||/\Sigma|F_{obs}|$.

R_{free} was calculated using 5% of data omitted from refinement.

Table 2

Dimerization kinetics of mB7H3 and mutants

Mutation	FG-Loop Sequence	Association Rate Constant $\times 10^{-5}$ ($L \cdot mol^{-1} \cdot s^{-1}$)
(wild-type)	IQDF	16.1±0.6
I126T	**T**QDF	4.1±0.1
F129A	IQD**A**	16.4±0.3
FG chimera	**YGGA**	0.83±0.08

*Values were determined using the fitting analysis shown in Fig. S3.